Vol. 580: 83–100, 2017
https://doi.org/10.3354/meps12310

MARINE ECOLOGY PROGRESS SERIES
Mar Ecol Prog Ser

Published September 29

Relationship between light, community composition and the electron requirement for carbon fixation in natural phytoplankton

Yuanli Zhu[1,*], Joji Ishizaka[1], Sarat Chandra Tripathy[2], Shengqiang Wang[3], Chiho Sukigara[4], Joaquim Goes[5], Takeshi Matsuno[6], David J. Suggett[7]

[1]Institute for Space-Earth Environmental Research, Nagoya University, Nagoya 464-8601, Japan
[2]ESSO-National Centre for Antarctic and Ocean Research, Ministry of Earth Sciences, Vasco-da-Gama, Goa 403804, India
[3]School of Marine Sciences, Nanjing University of Information Science and Technology, Nanjing, 210044, Jiangsu, PR China
[4]Graduate School of Environmental Studies, Nagoya University, Nagoya 464-8601, Japan
[5]Lamont-Doherty Earth Observatory at Columbia University, Palisades, New York 10964, USA
[6]Research Institute for Applied Mechanics, Kyushu University, Fukuoka 812-8581, Japan
[7]Climate Change Cluster, University of Technology Sydney, PO Box 123, Broadway, NSW 2007, Australia

ABSTRACT: Fast repetition rate fluorometry (FRRF) provides a means to examine primary productivity at high resolution across broad scales, but must be coupled with independent knowledge of the electron requirement for carbon uptake (K_C) to convert FRRF-measured electron transfer rate (ETR) to an inorganic carbon (C) uptake rate. Previous studies have demonstrated that variability of K_C can be explained by key environmental factors (e.g. light, nutrients, temperature). However, how such reconciliation of K_C reflects changes of phytoplankton physiological status versus that of community composition has not been well resolved. Therefore, using a dataset of coupled FRRF and C uptake measurements, we examined how the environmental dependency of K_C potentially varied with parallel changes in phytoplankton community structure. Data were combined from 14 campaigns conducted during the summer season throughout 2007 to 2014 in the East China Sea (ECS) and Tsushima Strait (TS). K_C varied considerably, but this variability was best explained by a linear relationship with light availability ($R^2 = 0.66$). Co-variability between K_C and light availability was slightly improved by considering data as 2 clusters of physico-chemical conditions ($R^2 = 0.74$), but was best improved as 2 taxonomic clusters: samples dominated by micro-phytoplankton (>20 µm) versus small phytoplankton (nano + pico, <20 µm; $R^2 = 0.70–0.81$). Interaction of phytoplankton community structure with light availability therefore explains the majority of variance of K_C. The algorithms generated through our analysis therefore provide a means to examine C uptake with high resolution from future FRRF observations from these waters.

KEY WORDS: Electron transfer rate · ETR · Primary productivity · Quantum requirement · Carbon fixation · Phytoplankton composition · Fast repetition rate fluorometry

INTRODUCTION

Fast repetition rate fluorometry (FRRF, Kolber et al. 1998) has been widely considered a key development for aquatic research in global efforts to better understand environmental regulation of primary productivity (Suggett et al. 2009b). A substantial number of studies have now demonstrated covariance between parallel measurements of FRRF-derived electron transport rates (ETRs) and C-uptake rates (e.g. Suggett et al. 2009a and references therein; Cheah et al. 2011, Robinson et al. 2014, Schuback et al. 2015), providing

*Corresponding author: zyl19840218@gmail.com

strong evidence that FRR fluorometers could potentially examine patterns of C uptake through application of an 'electron requirement for C-fixation' conversion factor (termed K_C; Lawrenz et al. 2013, Hancke et al. 2015). However, past parallel measurements of ETRs and C-uptake rates in fact show that K_C is highly variable since numerous factors can cause cellular processes to consume ETR-derived energy and reductant that is otherwise used for C assimilation (e.g. Lawrenz et al. 2013, Halsey & Jones 2015); consequently, use of an assumed constant for K_C is a likely cause for many FRRF-based overestimates of productivity rates (Kromkamp et al. 2008, Mino et al. 2014), in particular under excess irradiance (Ralph et al. 2010).

Recent research has investigated and modelled K_C variability in an attempt to better constrain FRRF-based estimates of phytoplankton C fixation. Lawrenz et al. (2013) synthesized global FRRF-based K_C data and demonstrated that this parameter could often be predicted as a function of key environmental factors that regulate phytoplankton productivity and community structure, notably light, temperature and inorganic nutrient availability. However, the specific relationship between these factors and K_C differed between oceanic regions of interest. More recently, Schuback et al. (2015, 2016) further demonstrated that K_C variance throughout iron-limited waters could be explained by co-variance with the extent of non-photochemical quenching (NPQ) status, interpreted as an indication of processes consuming photosynthetically derived energy and hence decoupling linear electron flow from C uptake. Whilst environmental regulation of K_C variability is clearly apparent, other studies noted that changes in phytoplankton community structure may contribute to this variance (see Suggett et al. 2006a, 2009a, Robinson et al. 2014). Such an observation is perhaps unsurprising where both ETR (e.g. Cermeño et al. 2005, Giannini & Ciotti 2016) and C-uptake rate (e.g. Tripathy et al. 2014, Barnes et al. 2015) vary across phytoplankton taxa, often as a first-order function of cell size, as a result of changes in prevailing hydrographic conditions. Variability of K_C across phytoplankton species has been examined for few laboratory cultures (Suggett et al. 2009a, Brading et al. 2013, Hoppe et al. 2015), and the potential influence of phytoplankton composition on K_C for natural field samples remains largely unexplored (Suggett et al. 2006a, Robinson et al. 2014).

To examine for the potential influence of phytoplankton community composition upon K_C variability, we analysed data from 14 experiments from 9 cruises conducted in the East China Sea (ECS) and Tsushima Strait (TS) over a period of 8 yr (2007–2014). The entire ECS and TS region is a very productive and highly dynamic region because of the seasonal fluctuation of several different water masses (Fig. 1). In summer, waters are characterized by high nutrient concentrations and elevated phytoplankton biomass (chlorophyll *a* [chl *a*]) in western regions as a result of the discharge from the Changjiang River (i.e. Changjiang diluted water, CDW), which constitutes about 85% of the total discharge by all rivers into the ECS (Ning et al. 1998). A pattern of depleted nutrients in parallel with low chl *a* is generally observed for the upper layer of the eastern ECS (Gong et al. 2003). Water mass for TS mainly originates from the ECS in summer (Guo et al. 2006) and is partly formed by the Kuroshio water, which flows northeastward along the eastern margin of the ECS continental shelf. Whilst CDW can potentially extend into TS, nutrients are likely depleted before reaching TS (Morimoto et al. 2009). As such, the bio-optical properties as well as phytoplankton size structure appear notably different between TS and the ECS (Wang et al. 2014), providing an ideal study region to examine variability in K_C.

We recently reported a strong, but non-linear, correlation between parallel measured FRRF-based ETRs and C-uptake rates for a semi-enclosed bay (Ariake Bay). Variance of K_C derived from these parallel measurements appears largely explained by light availability (Zhu et al. 2016). However, phytoplankton community composition remained generally unchanged throughout the Ariake Bay dataset, and as yet it is unclear whether this light-dependent regulation of K_C is potentially further influenced by the dominant phytoplankton species present. To test for this potential influence, we therefore specifically examined parallel FRRF measurements and 24 h on-deck ^{13}C incubations from the ECS and TS that were collected under diverse prevailing environmental conditions (e.g. light, nutrients) as well as phytoplankton community structure. We specifically (1) tested whether light-dependent variability of K_C (derived from 24 h on-deck ^{13}C uptake) observed for Ariake Bay was similarly observed across the broader biogeographic domain of the ECS and TS; and (2) evaluated the extent to which the phytoplankton community structure, as determined from high performance liquid chromatography (HPLC), further influenced the environmental dependency of K_C. Together we used these data to further develop a specific K_C algorithm for this region and hence a practical FRRF-based method for more broadly examining C-uptake dynamics in the ECS and TS.

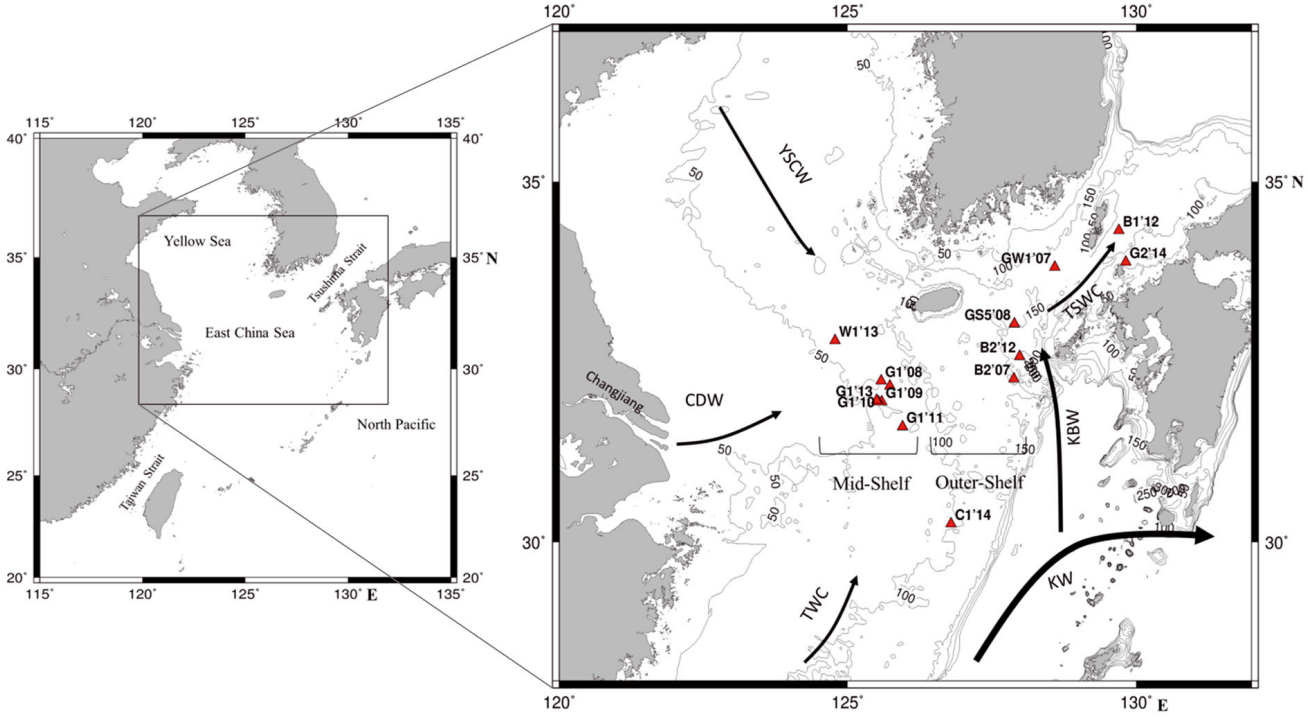

Fig. 1. Study area and sampling locations. Main currents during the summer period are also shown: Kuroshio Water (KW), Kuroshio Branch Water (KBW), Taiwan Warm Current (TWC), Yellow Sea Cold Water (YSCW), Tsushima Strait Warm Current (TSWC) and Changjiang Diluted Water (CDW) (Ichikawa & Beardsley 2002). Light gray lines indicate the isobaths (in m). The numbers shown beside each station name represent year of the cruise when the station was sampled. G1′10 contains 2 sampling points, G1-1′10 and G1-2′10, at the same location

MATERIALS AND METHODS

Sampling area, sites and dataset

Analysed datasets were from 14 (12 for parallel measured ^{13}C-ETR) campaigns conducted across the ECS and TS region (Fig. 1) during the summers of 2007–2014 (Table 1). Water mass interactions in this region are complex and in summer are influenced by CDW from the east, the Taiwan Warm Current from the south, the Kuroshio Branch Water from the west and the Yellow Sea Cold Water from the north (Fig. 1).

Table 1. Stations, geographical locations, time of sampling and environmental characteristics during the sampling campaigns. PAR: photosynthetically active radiation, MLD: mixed layer depth, DCM: deep chlorophyll *a* maximum, Z_{eu}: euphotic depth (depth with 1% of surface PAR), FRRF: fast repetition rate fluorometry, NA: not applicable

No.	Date	Station	Location	Daily PAR (E_0^+, mol quanta m^{-2} d^{-1})	MLD (m)	Depth of DCM (m)	Z_{eu} (m)	FRRF observation periods (h)
1	23 July 2007	GW1′07	33.84° N, 128.59° E	60.2	14	34	60	6:00 – 10:00
2	26 July 2007	B2′07	32.3° N, 127.88° E	59.5	10	65	85	6:00 – 18:00
3	25 July 2008	GS5′08	33.06° N, 127.89° E	50.4	13	42	65	6:00 – 10:00
4	11 Aug 2008	G1′08	32.27° N, 125.58° E	44.4	10	NA[b]	22	6:00 – 18:00
5	20 July 2009	G1′09	32.27° N, 125.59° E	28.6	4	13	26	4:00 – 16:00
6	19 July 2010	G1-1′10	31.98° N, 125.53° E	58.0	6	20	35	4:00 – 16:00
7	23 July 2010	G1-2′10	32.2° N, 125.73° E	48.2	4	20	35	4:00 – 16:00
8	21 July 2011	G1′11	31.63° N, 125.95° E	42.9	2	30	35	4:00 – 16:00
9[a]	22 July 2012	B1′12	34.34° N, 129.7° E	51.2	8	43	47	4:00 – 16:00
10[a]	25 July 2012	B2′12	32.61° N, 127.98° E	43.3	5	57	70	4:00 – 16:00
11	23 July 2013	G1′13	32.0° N, 125.5° E	32.8	10	30	32	4:00 – 10:00
12	26 July 2013	W1′13	32.83° N, 124.78° E	19.1	4	10	21	4:00 – 18:00
13	21 July 2014	C1′14	30.26° N, 126.79° E	65.0	5	42	55	6:00 – 18:00
14	26 July 2014	G2′14	33.91° N, 129.82° E	55.3	2	40	50	6:00 – 18:00

[a]No ^{13}C data; [b]maximum chl *a* was within the upper mixed layer

Stations for conducting parallel FRRF and C-uptake rate measurements were located in 3 sub-areas of this region: the mid-shelf of the ECS, outer-shelf of the ECS and the TS (Fig. 1, Table 1).

Sampling and measurements of physical and biochemical properties

Sampling protocols for all parameters and ^{13}C experiments employed in our study are similar to those reported previously (Siswanto et al. 2006, Wang et al. 2014, 2015; see also Zhu et al. 2016 for Ariake Bay). Seawater samples for ^{13}C-uptake experiments for all cruises were collected before sunrise, from 6 depths corresponding to light levels of approximately 100, 50, 25, 10, 5 and 1% of the surface photosynthetically active radiation (PAR, 400–700 nm, measured in µmol quanta m^{-2} s^{-1}). Water was sampled using a rosette equipped with 12 Niskin bottles (5 l capacity; General Oceanics) and a conductivity-temperature-depth profiler (911+, SeaBird Electronics). Sampling depths were determined by a high-resolution profiling reflectance radiometer (PRR-800/810, Biospherical Instruments) profile conducted 1 d prior to incubations. Incident PAR at the sea surface (E_0^+) was measured throughout the sample incubating period with a quantum scalar irradiance sensor (QSL-2100, Biospherical) mounted on the incubators. *In situ* underwater irradiance field $E_d^-(\lambda,z)$ was measured during the incubation period for 13 wavelengths (λ = 380, 412, 443, 465, 490, 510, 532, 555, 565, 589, 625, 665 and 683 nm) using the PRR-800 profiled every 2 h from 10:00 to 16:00 h (local time), from the surface to the euphotic depth (Z_{eu}, defined as the depth with 1% of surface PAR). Repeated profiles were conducted every 2 h, according to a Lagrangian approach, via a buoy track to enable repeat measurements on the same water mass.

Seawater samples were processed as follows for chl *a*, nutrients and phytoplankton light absorption measurements. An aliquot of 100 ml seawater was filtered onto 25 mm glass fibre filters (Whatman GF/F) under low vacuum pressure (<0.02 MPa) to determine chl *a* content. Filters were extracted in N, N-dimethylformamide for 24 h in darkness at −20°C (Suzuki & Ishimaru 1990), and chl *a* was quantified using a pre-calibrated fluorometer (10-AU, Turner Design). A second aliquot of 5 ml for nitrate + nitrite (NO_x^-), phosphate (PO_4^{3-}) and silicate (DSi) analyses was stored at −20°C until later analysis using an automated nutrient analyser (AACS-IV, BL-TEC; and TRAACS 2000, Bran+Luebbe). Detection limits based on this approach were 0.1, 0.08 and 0.1 µM for NO_x^-, PO_4^{3-} and DSi, respectively.

Phytoplankton particulate absorption coefficients, $a_{ph}(\lambda)$ (m^{-1}), were determined from a 500 ml aliquot using the quantitative filter technique of Cleveland & Weidemann (1993) as adapted by Wang et al. (2014). Wavelength-resolved phytoplankton absorption spectra were determined as $a_{ph}(\lambda) = a_p(\lambda) - a_{np}(\lambda)$, where a_p and a_{np} refer to total particulate material and non-phytoplankton particles. The chl *a*-specific absorption coefficient, $a^*_{(ph)}(\lambda)$ (m^2 [mg chl *a*]$^{-1}$), was then calculated as $a_{ph}(\lambda)$ normalised to the corresponding chl *a* concentration.

Additional aliquots of 1 l water samples were again filtered onto 25 mm GF/F filters under low vacuum pressure (<0.02 MPa), and immediately frozen in liquid nitrogen and stored at −80°C for later laboratory analysis. Samples were analysed by reverse-phase HPLC with a Zorbax Eclipse XDB-C8 column (150 mm × 4.6 mm, 3.5 µm; Agilent Technologies), and 19 pigments were separated and quantified following the method of Van Heukelem & Thomas (2001).

Measurements of C uptake were carried out via 24 h on-deck simulated *in situ* incubations with enrichment of ^{13}C stable isotope (min 98 atom%; $NaH^{13}CO_3$, ISOTEC), where the final ^{13}C atom% of total dissolved inorganic C was ca. 10% of that in the ambient water (Hama et al. 1983). Sampling depths for incubation corresponded to 100, 50, 25, 10, 5 and 1% of PAR measured just below the sea surface (E_0^-), which were determined by PRR-800 measurements 1 d before at the same location. Incubators that simulated the irradiance levels from 50 to 1% of surface values were covered with blue plastic filters (General Environmental Technos) to achieve the desired irradiances (no filter was used for the 100% PAR incubator). Sampling, experimental procedures and in-lab measurements were the same as described previously by Tripathy et al. (2010) and Zhu et al. (2016), except that the sampling volume was 1 l for this region. Finally, C fixation rates ($P^C[z]$) were calculated according to Hama et al. (1983) as follows:

$$P = \frac{\Delta C}{t} = \frac{C \times (a_{is} - a_{ns})}{t \times (a_{ic} - a_{ns})} \quad (1)$$

where P is the photosynthetic rate (mgC m^{-3} d^{-1}), t is the time of incubation in hours (for our study, 24 h), C is particulate organic C (POC) in the incubated sample (mgC m^{-3}), ΔC is POC increase during the incubation (mgC m^{-3}), a_{is} is the atomic% of ^{13}C in the incubated sample, a_{ns} is the atomic% of ^{13}C in the natural sample, and a_{ic} is the atomic% of ^{13}C in the total inorganic C. All ^{13}C data (P; Eq. 1) were

subsequently spectrally corrected to account for the differences between light spectra for the incubators versus those *in situ*. For this, values of P were adjusted by the ratio $\overline{a}^{chl}(in\ situ)/\overline{a}^{chl}$(incubator), where $\overline{a}^{chl}$(incubator) and $\overline{a}^{chl}(in\ situ)$ represent the phytoplankton absorption coefficients weighted to the irradiance spectra in each incubator and irradiance spectra *in situ*, respectively. Chl *a* specific primary productivity ($P^C_B(z)$) was calculated as $P^C(z)$ divided by chl *a* concentration, and the water column integrated $P^C(PP_{eu})$ was derived as $\int_0^{Zeu} P^C(z)dz$.

Phytoplankton pigment-based size fractionation

In order to consider the taxonomic nature of the phytoplankton community, we employed diagnostic pigment (DP) analysis following Vidussi et al. (2001) and Uitz et al. (2006) to estimate the respective contribution of 3 phytoplankton size classes: pico- (<2 µm), nano- (2–20 µm) and micro-phytoplankton (>20 µm) to total chl *a* (Tchl*a*) biomass. Their approach uses 7 biomarker pigments (fucoxanthin [Fuco], peridinin [Per], 19′-hexanoyloxyfucoxanthin [Hex], 19′-butanoyloxyfucoxanthin [But], alloxanthin [Allo], chlorophyll *b* [chl *b*] and zeaxanthin [Zea]). Hirata et al. (2008) further revised the approach to account for the occurrence of chl *b* in larger eukaryotes such as chlorophytes. We therefore followed Hirata et al. (2008), subsequently adapted by Wang et al. (2014), for phytoplankton size fraction analysis for the same region as in our study. The fraction of each size class was expressed as:

$$f_{micro} = (1.41Fuco + 1.41Per) / \Sigma DP \quad (2)$$

$$f_{nano} = (0.60Allo + 0.35But + 1.27Hex + 1.01chl\ b) / \Sigma DP \quad (3)$$

$$f_{pico} = 0.86Zea / \Sigma DP \quad (4)$$

$$\Sigma DP = 1.41Fuco + 1.41Per + 0.60Allo + 0.35But + 1.27Hex + 1.01chl\ b + 0.86Zea \quad (5)$$

where coefficients for ΣDP follow Wang et al. (2014). Based on their approach, f_{micro}, f_{nano} and f_{pico} represent the fraction of relatively large diatoms and dinoflagellates; the fraction of relatively smaller prymnesiophytes, chrysophytes, cryptophytes and chloropytes; and the fraction of cyanobacteria only, respectively.

FRRF measurements, ETR and K_C

In parallel with the 24 h deck-board ^{13}C-uptake measurements and the *in situ* multispectral irradiance profiles, we also conducted FRRF fluorescence profile measurements every 2 h from dawn to dusk (as per Zhu et al. 2016). For 3 of the sampling campaigns, these diurnal FRRF profiles could only be conducted for half the daylight period and therefore are treated separately, as described below. Fluorescence inductions were performed semi-continuously from the near surface (~1 m deep) to depths $>Z_{eu}$ using a Diving Flash FRRF (Kimoto Electric). The instrument is equipped with both dark and light chambers as well as an integrated scalar PAR sensor (QSP-2200, Biospherical). The FRRF was deployed with an initial 1 min stop at the surface and a subsequently low profiling speed (<0.2 m s^{-1}) to ensure acquisition of fine-scale surface and vertically resolved active fluorescence data (as per Mino et al. 2014). Settings for each FRRF induction acquisition followed Fujiki et al. (2008). Each induction transient was then fitted to the biophysical model of Kolber et al. (1998) to determine the minimum fluorescence yield, maximum fluorescence yield, effective absorption and photochemical efficiency of photosystem II (PSII) from both dark (F_o, F_m, σ_{PSII} and F_v/F_m, respectively) and light (F', F_m', σ_{PSII}', F_q'/F_m', respectively) chambers, using custom software (FRRCalc2, Kimoto Electric). From these FRRF parameters, and in concert with the *in situ* and on-deck irradiance measurements, we used the approach of Zhu et al. (2016) to determine the daily-integrated ETR. Firstly, we calculated the instantaneous PSII reaction centre (RCII) normalised ETR, ETR_{RCII} (mol e^- [mol RCII]$^{-1}$ s^{-1}) per depth (z, m) and measurement time (t, h) from the FRRF profiles as:

$$ETR_{RCII}(z,t) = PAR(z,t) \times \sigma^{470}_{PSII}(z,t) \times q_p(z,t) \times \Phi_{RC} \times 6.022 \times 10^{-3} \quad (6)$$

where PAR is in units of µmol quanta m^{-2} s^{-1}, and σ^{470}_{PSII} is the spectrally uncorrected effective absorption cross section of PSII from the dark chamber (Å^2 quanta^{-1}). Note that under ambient light conditions, σ^{470}_{PSII} from the dark chamber accounts for any non-rapidly reversible (>s) non-photochemical quenching associated with the antennae (e.g. Suggett et al. 2006a,b). Φ_{RC} accounts for the assumption that 1 electron is produced from each RCII charge separation (see Kolber & Falkowski 1993). The constant value 6.022×10^{-3} converts µmol quanta to quanta, RCII to mol RCII and Å^2 to m^2. Finally, the term q_p (dimensionless) is the PSII operating efficiency and accounts for the extent of photochemical energy conversion by RCIIs, determined as the ratio of apparent PSII photochemical efficiency measured in 'light' and 'dark' chambers of the

FRRF, following the procedure of Suggett et al. (2006a,b):

$$q_p = \frac{(F_{max} - F_{min})/(F_{max} - f)_{light\ chamber}}{(F_{max} - F_{min})/(F_{max} - f)_{dark\ chamber}} \quad (7)$$

Importantly, this procedure overcomes the need to correct the PSII efficiency with knowledge of a fluorescence blank since the contribution of the blank (f) will be identical for both light and dark chambers and thus cancel (Suggett et al. 2006a).

We next constructed an ETR_{RCII} versus PAR relationship for each of the 6 light depths used for the corresponding incubations from profiles conducted across each sampling day (6–7 casts d^{-1}). Here, ETR_{RCII} and PAR data were binned per light depth and fit to the photosynthesis-light dependency model of Jassby & Platt (1976), Eq. (8). For the 3 campaigns where data were collected during half of the daylight period only, the ETR_{RCII} versus PAR relationship was constructed by combining profiles data from all 3 FRRF casts together and applied to each of the 6 depths. In this way, we were also able to get a general ETR_{RCII}–PAR relationship for sampling campaigns where not enough FRRF data were obtained for depth-specific ETR_{RCII}–PAR curve construction.

$$ETR(z,t) = ETR_{max} \times \tanh\left(\frac{\alpha PAR(z,t)}{ETR_{max}}\right) \quad (8)$$

For waters where light saturation for ETR_{RCII} versus PAR was not observed, and hence ETR_{RCII} remained light dependent, simple linear regression was instead used to describe the light-dependency of ETR_{RCII} (i.e. the slope is equivalent to α). Relationships between ETR_{RCII} and PAR for samples obtained under light-saturation and light-limiting conditions are provided in Fig. S1 in the Supplement (at www.int-res.com/articles/suppl/m580p083_supp.pdf) as examples. Using knowledge of α and/or ETR_{max}, we were then able to retrieve the ETR_{RCII} for any given value of PAR over depth and time.

$PAR(z,t)$ was specifically determined for our 6 sampling depths and derived from continuously measured incident PAR at the surface $PAR(0^+)$. The factor 0.9 was used to convert PAR above the water surface relative to that just beneath the surface ($PAR[0^-]$; see Marra 2015). In water, PAR at the % light depth of interest (x%) could be determined as $PAR(0^-)(t) \times x$% (see Zhu et al. 2016). Knowledge of $PAR(t,z)$ could then be applied to Eq. (5) to retrieve ETR for the given depths and time, $ETR(z,t)$. Daily integrated ETR_{RCII} (mol e^- [mol RCII]$^{-1}$ d^{-1}) for each specific depth was finally determined as:

$$\text{daily } ETR_{RCII}(z) = \int_{t1}^{t2} ETR_{RCII}(z,t)\,dt \quad (9)$$

In order to convert ETR normalised to RCII content (ETR_{RCII}) to that normalised to chl a content, and hence ETRs that could be directly compared with parallel measures of C uptake to retrieve K_C (Lawrenz et al. 2013), knowledge of the RCII per chl a (i.e. n_{PSII}, mol RCII [mol chl a]$^{-1}$) is required. Direct measurement of n_{PSII} under natural conditions is extremely challenging (Moore et al. 2006, Suggett et al. 2006a), often requiring that the RCII concentration be determined indirectly (see Suggett et al. 2010). Based on previously published information, we employed an approach to determine n_{PSII} based on phytoplankton taxonomic size class information. We summarized n_{PSII} from 11 phytoplankton species under various growth conditions (reported by Suggett et al. 2004) and grouped this dataset into 2 size communities; <2 µm (cyanobacteria) with n_{PSII} of 0.0038 ± 0.00004 mol RCII (mol chl a)$^{-1}$ and >2 µm (other eukaryotes) with average (±SE), n_{PSII} of 0.0017 ± 0.00003 mol RCII (mol chl a)$^{-1}$, respectively. Thus, n_{PSII} was calculated based on size fraction derived from HPLC, using the following equation:

$$n_{PSII} = \%(\text{Micro} + \text{Nano}) \times 0.0017 + \%(\text{Pico}) \times 0.0038 \quad (10)$$

Measurements of σ_{PSII} were weighted to the narrow blue excitation waveband (470 nm) used for fluorescence induction by the FRRF. To therefore account for the spectral differences between FRRF-LEDs and the natural light spectra *in situ*, we employed a σ_{PSII}-correction factor (F) according to Eq. (11) following Suggett et al. (2006b):

$$F = \sigma^{abs}_{PSII} / \sigma^{470}_{PSII} = \left(\frac{\bar{a}^{chl}_{in\ situ}}{\bar{a}^{chl}_{FRRF}}\right) \quad (11)$$

where σ^{abs}_{PSII} represents spectral corrected σ_{PSII}; $\bar{a}^{chl}_{FRRF}$ and $\bar{a}^{chl}_{in\ situ}$ represent the absorption coefficients weighted to the FRRF excitation spectra and *in situ* irradiance spectra, respectively. Detailed calculations for $\bar{a}^{chl}_{FRRF}$ and $\bar{a}^{chl}_{in\ situ}$ can be found in Suggett et al. (2004) and Zhu et al. (2016). A daily chl a-specific ETR at light depth (z) (mmol e^- [mg chl a]$^{-1}$ d^{-1}) was thus calculated as follows:

$$\text{daily } ETR(z) = \text{daily } ETR_{RCII}(z) \times n_{PSII} \times F \times 893^{-1} \quad (12)$$

where the constant factor 893 converts mol chl a to mg chl a and mol e^- to mmol e^-.

Finally, K_C (mol e^- [mol C]$^{-1}$) was defined to be the ratio of the 2 independently determined variables, ETR and P^C_B as per Zhu et al. (2016):

$$K_C(z) = [\text{daily } ETR(z)]/[P^C_B(z)] \times 12 \quad (13)$$

where P^C_B is the daily-integrated C assimilation per unit chl *a* (mgC [mg chl *a*]$^{-1}$ d^{-1}), and the factor 12 converts g C to mol C.

Statistical analyses

Hierarchical cluster analysis (HCA) was applied to physico-chemical parameters across sampling campaigns for grouping into common hydrographic conditions, and the 'ward.D2' method in R was adopted for running HCA, using Euclidean distances as input dissimilarities (Murtagh & Legendre 2014). Spearman rank correlation analysis and stepwise regression were used to examine the contribution of physico-chemical (or taxonomic) variables in explaining variance of K_C. A Kolmogorov-Smirnov test was used to examine data normal distribution. Welch's *t*-test and ANCOVA were applied to test for significant differences between cluster or group data and the linear regression models. All statistical analyses and curve fitting were performed using the open-source statistical software R version 3.2.3 (R Core Team 2014).

RESULTS

Variability of C uptake rates, ETRs and K_C

Volume-normalised C uptake rates ($P^C(z)$, mgC m^{-3} d^{-1}) across all sampling campaigns were generally higher for the ECS mid-shelf than for ECS outer shelf and TS waters (Table 2), and reflected that phytoplankton biomass was also higher for the ECS mid-shelf than the ECS outer shelf/TS. Specifically, surface mean P^C and chl *a* was ca. 10 times (upper mixed layer) or 4 times (deep chl *a* maximum, DCM) higher for the ECS mid-shelf than the ECS outer-shelf/TS, whereas values for chl *a*-normalised $P^C(P^C_B(z))$ were generally equivalent across sites for both the upper mixed layer (ca. 40 mgC [mg chl a]$^{-1}$ d^{-1}) and DCM (ca. 20–30 mgC [mg chl a^{-1}] d^{-1}). Euphotic depth integrated $P^C(PP_{eu})$ values ranged from 330 to 1250 mgC m^{-2} d^{-1} across the study area, but were overall higher for the ECS mid-shelf with (mean ± SE) 853 ± 97 mgC m^{-2} d^{-1} compared to ECS outer-shelf/TS (451 ± 51 mgC m^{-2} d^{-1}).

Significant variability of ETR_{RCII} was observed over the course of the diurnal cycle, with patterns of ETR_{RCII} closely coupled with surface PAR over time (e.g. ETR_{RCII} of surface and DCM, Fig. 2); as expected, this ETR_{RCII} variability was dampened at depth (DCM) as a result of the lower light availability. Thus for any given light depth, values of daily integrated ETR(*z*) were therefore closely correlated with those of daily integrated PAR(*z*) across all sampling campaigns (R^2 = 0.93, n = 72, p < 0.001), with a maximum value of ca. 170 mmol e$^-$ (mg chl *a*)$^{-1}$ d^{-1} (Fig. 3a) from across the entire dataset. In contrast, greater non-linearity (and in effect, daily light saturation) was observed when parallel values for the daily-integrated rate of C uptake ($P^C_B(z)$) were plotted against PAR(*z*) (Fig. 3b). Given the respective patterns of light dependency for ($P^C_B(z)$) and ETR(*z*), further plotting of $P^C_B(z)$ against corresponding values of ETR(*z*) highlighted non-linearity between corresponding data points (Fig. 3c) and thus a clear indication that the electron requirement for C fixation (K_C, ETR(*z*)/$P^C_B(z)$) was not constant. Overall, K_C (mol e$^-$ [mol C]$^{-1}$) ranged from values of 1.0 to 66.5 mol e$^-$ (mol C)$^{-1}$, similar to values reported for a previously synthesized global K_C dataset (Lawrenz et al. 2013).

Of our 67 K_C data points, 8 values (primarily from PAR depths of 5 and 1% $E(0^-)$), were below the theoretical minimum of 4 mol e$^-$ (mol C)$^{-1}$. K_C values <4 have been previously observed for laboratory cultures under controlled conditions but only where ambient light levels are lowest. Therefore, considering the low values of P^C_B at these light depths (mean ± SD, 11.6 ± 10.2 mgC [mg chl *a*]$^{-1}$ d^{-1}) and their relatively small proportion to the whole dataset, we excluded K_C values <4 mol e$^-$ (mol C)$^{-1}$ from further analysis, as a result of possible inaccuracies associated with very low light C-uptake rates (Cullen 2001) or errors in n_{PSII}. With the exclusion of these 8 data points, K_C varied from 4.3 to 66.5 mol e$^-$ (mol C)$^{-1}$ with a mean ± SD of 19.8 ± 14.2 mol e$^-$ (mol C)$^{-1}$.

Table 2. Means (± SE) of chl *a* normalised primary productivity (P^C_B, mg C [mg chl *a*]$^{-1}$ d^{-1}) and volume-normalised primary productivity (P^C, mgC m^{-3} d^{-1}) measured for the upper mixed versus deep chlorophyll maxima (DCM) water, as well as column-integrated primary productivity (PP_{eu}, mgC m^{-2} d^{-1}; where PP_{eu} refers to $P^C(z)$ integrated from the surface to the euphotic depth [depth with 1% of surface PAR]) of 2 main study regions (ECS: East China Sea; TS: Tsushima Strait

Region	Layer	P^C_B	P^C	PP_{eu}
ECS mid-shelf (n = 7)	Upper mixed layer	41.5 (4.6)	51.5 (7.2)	853 (97)
	DCM Layer	19.4 (8.2)	31.0 (8.5)	
ECS outer-shelf & TS (n = 5)	Upper mixed layer	43.9 (5.3)	5.4 (0.5)	451 (51)
	DCM Layer	16.2 (2.4)	10.1 (2.1)	

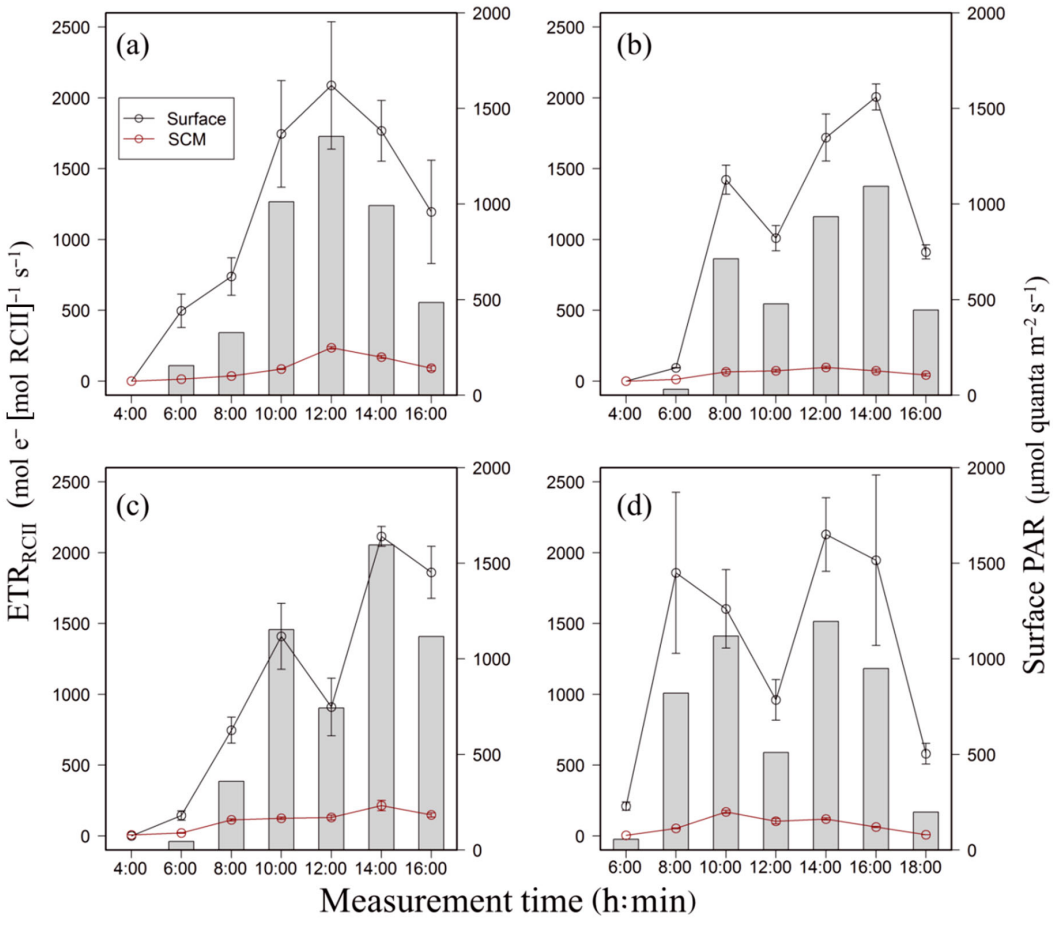

Fig. 2. Four examples of time series of electron transport rate (ETR_{RCII}, mol e^- [mol RCII]$^{-1}$ s^{-1}, where RCII is the reaction centre of photosystem II) at the surface (black circles) and subsurface chlorophyll *a* maximum (SCM, red circles) with surface instantaneous photosynthetically active radiation (PAR, gray bars). Data from Stations (a) G1-2'10, (b) G1'11, (c) B1'12 and (d) G2'14 are presented (see Fig. 1 for station locations). Vertical bars indicate the standard deviations of data included in the upper mixed and SCM layer, respectively

Resolving variability of K_C via changes in light intensity

Spearman rank analysis of K_C for different environmental factors yielded PAR with the highest correlation coefficient with K_C (Spearman, r = 0.82, p < 0.001, see Table S1 in the Supplement). Stepwise regression further confirmed that PAR alone explained most (66%) of K_C co-variability (Table S2 in the Supplement). PAR was therefore considered to be the main factor explaining the variability of K_C for this region. Indeed, variability of K_C for the entire dataset could therefore be described by a simple PAR-dependent linear model (K_C = 0.85PAR + 6.55, R^2 = 0.66, n = 59, p < 0.001, Fig. 3d) as we have demonstrated previously for Ariake Bay (Zhu et al. 2016). We further considered whether K_C variability was different for (high light) upper mixed layers compared to the (lower light) other depths. Binning K_C values into these 2 sample groups demonstrated that K_C was higher and much more variable in the upper mixed layer (mean ± SE, 31.2 ± 3.3 mol e^- [mol C]$^{-1}$) compared to the other depths (13.2 ± 1.1 mol e^- [mol C]$^{-1}$; see Fig. 3d).

Resolving variability of K_C via changes in phytoplankton community structure

Sampling stations analysed by HCA based on prevailing physico-chemical features (sea surface temperature, salinity and nutrients [NO_3^-+NO_2^-, PO_4^{3-}], water column mixed layer depth [MLD] and mean light diffuse attenuation K_d[PAR]) yielded 2 main groups (Fig. 4a). Specifically, stations were clustered (Cluster 'A', most located in the outer shelf and TS) with higher salinity, lower nutrient and chl *a* concentrations compared to all other stations ('Cluster 'B';

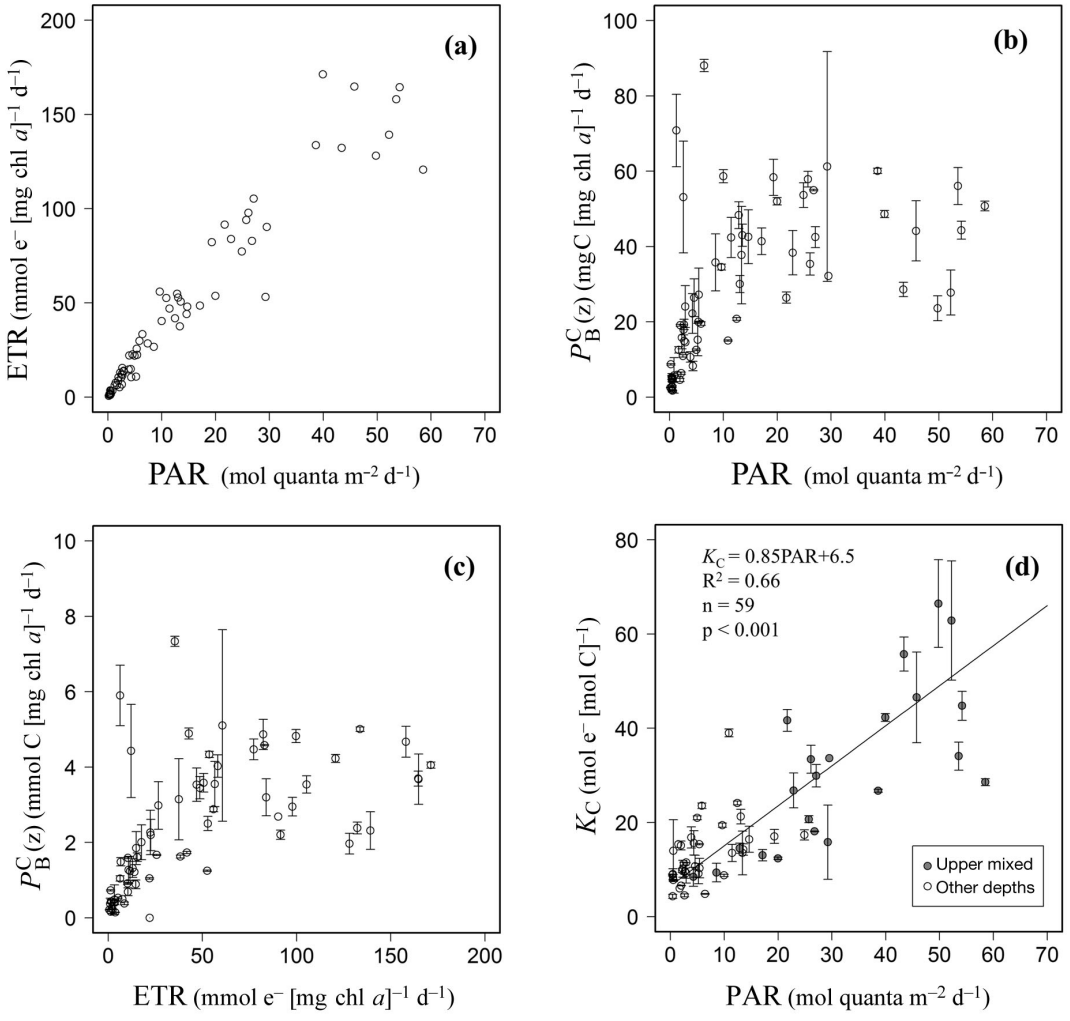

Fig. 3. (a) All data of daily electron transport rate (ETR) versus daily photosynthetically active radiation (PAR). (b) Chl *a* normalised primary productivity ($P^C_B(z)$) versus daily PAR. (c) $P^C_B(z)$ versus daily ETR. (d) K_C (electron requirement for C-fixation) versus daily PAR for data divided into upper mixed layer (gray) and other depths (white).Vertical bars represent standard deviations of P^C_B and K_C from 3 replicates for each sampling depth. Type II linear regression was fitted for all data in panel (d)

Table 3). Analysis of the phytoplankton community structure revealed dominance by f_{pico} (%, mean ± SE, 45.7 ± 7.5) or f_{micro} (41.2 ± 6.3) for stations comprising Clusters A and B, respectively (Table 3). However, these 2 clusters also exhibited similar proportions of f_{nano} (43 vs. 32%, respectively). Mean (± SE) values for K_C within this high-light upper mixed layer was similar for data binned according to these 2 clusters (28.7 ± 1.6, n = 10; vs. 34.1 ± 4.2 mol e^- [mol C]$^{-1}$, n = 16; Table 3). Based on this HCA result, we plotted PAR(z) versus $K_C(z)$ for these 2 clusters separately to further examine the potential influence of environmental conditions on the light-dependency of K_C (Fig. 4b). Here, the correlation between $K_C(z)$ and PAR(z) was improved (R^2 = 0.74, Fig. 4b) for both clusters compared to that previously where all data were pooled (R^2 = 0.66, Fig. 3d). Furthermore, Cluster B data exhibited a significantly higher regression slope than Cluster A (1.1 vs. 0.55, ANCOVA, df = 1, p < 0.001; Fig. 4b).

Given the substantial overlap of phytoplankton group dominance between physico-chemical defined clusters (and the focus on only the upper mixed layers), we subsequently re-binned all data across all campaigns/depths according to the dominant phytoplankton fraction. This approach yielded dominant phytoplankton size groups (f_{micro}-, f_{nano}- and f_{pico}-dominated) consisting of 26, 20 and 13 data points, respectively (Table 4). Mean $K_C(z)$ was again effectively constant (ca. 16–22 mol e^- [mol C]$^{-1}$) across these 3 phytoplankton size bins (Table 4), although median $K_C(z)$ values were generally higher for f_{pico}

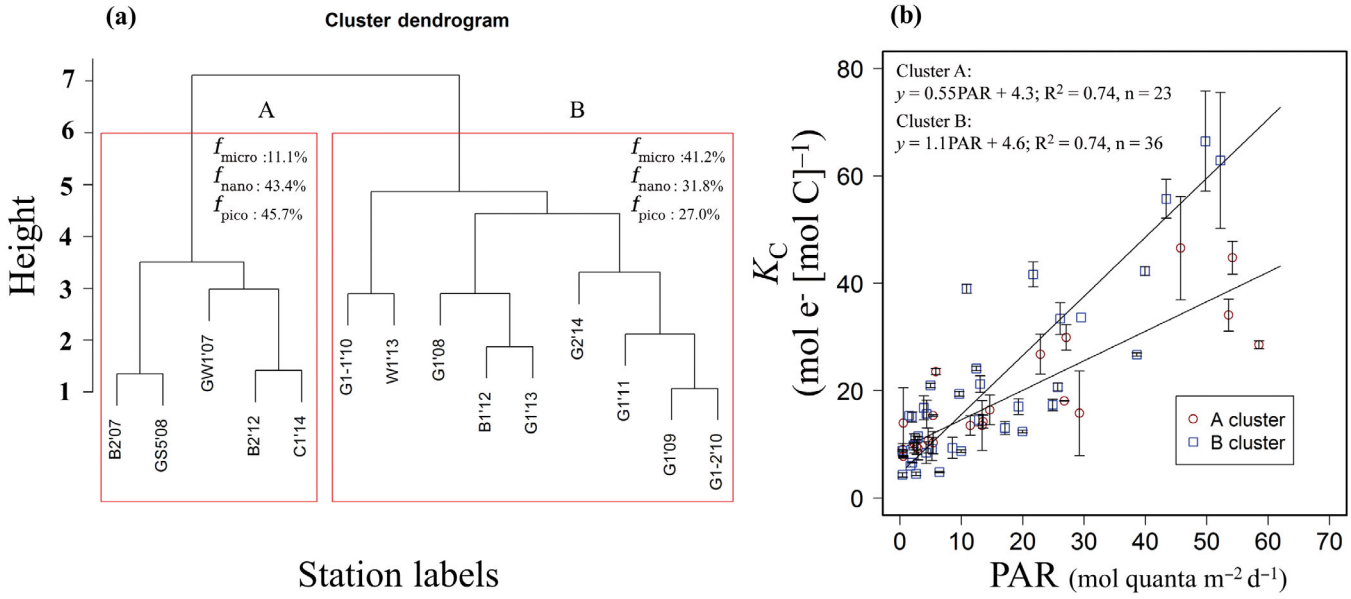

Fig. 4. (a) Hierarchical cluster analysis (HCA) of stations based on relative contribution of physicochemical parameters (sea surface temperature, salinity, NO_3^-+NO_2^-, PO_4^{3-}, mixed layer depth and light diffuse attenuation). Result of HCA identified 2 main clusters, A and B. (b) Daily photosynthetically active radiation (PAR) and K_C (electron requirement for C-fixation) for the 2 clusters separately. Equations are from Type II linear regressions: all $p < 0.001$

compared to f_{nano} or f_{micro} (ca. 18 compared to ca. 15 or 12, Fig. 5a). Such higher K_C values for f_{pico}-dominated waters may be a function of the higher n_{PSII} values ascribed to these waters (Suggett et al. 2004), or the higher light intensity since most f_{pico}-dominated waters were at the surface (Lawrenz et al. 2013). Re-evaluating the relationship of $K_C(z)$ versus PAR(z) in terms of these 3 size bins (Fig. 5b) improved the extent of covariance that could be explained (R^2 = 0.59–0.81, $p < 0.001$) compared to the pooled data (Fig. 3d) or, in the case of f_{micro} and f_{pico}, compared to the 2 physico-chemical based clusters (Fig. 4b). ANCOVA analysis demonstrated that the regression slopes describing the relationship between K_C and PAR for f_{micro} was significantly different than for f_{nano} and f_{pico} (df = 1, $p < 0.001$) but not for f_{nano} compared to f_{pico} (df = 1, $p = 0.2$; Fig. 5b). Thus, data from f_{nano} and f_{pico} bins were pooled for final analysis. Overall, the linear regression slope of $K_C(z)$ versus PAR(z) was higher by a factor of ca. 2 for samples dominated by micro-phytoplankton (i.e. f_{micro} > 20 µm, determined by pigments of Fuco and Per) than those dominated by small phytoplankton (f_{nano} + f_{pico}, <20 µm, determined by pigments of Hex, But, Allo, chl *b*, and Zea; slope: 1.2 vs. 0.56, ANCOVA, df = 1, $p < 0.001$). Considering the data as these 2 different taxonomic groups demonstrated improved correlation between $K_C(z)$ and PAR(z) (R^2 = 0.70–0.81, Fig. 5c) compared to physico-chemical defined clusters (0.74; Fig. 4b), suggesting that K_C appears primarily influenced by light and secondarily by dominant phytoplankton taxa present. These improved regression coefficients for taxonomic-based groups suggest that accounting for differences in phytoplankton community composition is therefore important in these waters for improving light-dependent estimations of K_C across broad environmental regimes such as those seen here in the ECS.

Table 3. Means (± SE) of environmental parameters and phytoplankton size fractions constituting phytoplankton populations, and values of K_C (electron requirement for C-fixation) of the upper mixed layer populations within Clusters A (n = 9) and B (n = 15) (see Fig. 4). Welch's *t*-test results are shown comparing the differences between the 2 clusters. Values in **bold** indicate significant correlations at $p < 0.05$

Cluster	Temp. (°C)	Sal.	NO_x^- (µM)	PO_4^{3-} (µM)	N:P	Chl *a* (mg m^{-3})	Micro (%)	Nano (%)	Pico (%)	K_C (mol e$^-$ [mol C]$^{-1}$)
A	26.9 (0.6)	33.3 (0.3)	0.02 (0.01)	0.01 (0.01)	2.3 (0.9)	0.13 (0.02)	11.1 (3.6)	43.4 (5.6)	45.7 (7.5)	28.7 (1.6)
B	26.5 (0.3)	30.5 (0.4)	0.45 (0.15)	0.08 (0.02)	13.9 (7.1)	1.16 (0.25)	41.2 (6.3)	31.8 (3.0)	27.0 (4.7)	34.1 (4.2)
p	0.5	**0.001**	0.07	**0.02**	0.3	**0.02**	**0.007**	0.1	0.06	0.7

Table 4. Means (± SE) of phytoplankton size composition (%) and associated K_C (electron requirement for C-fixation) values (mol e^- [mol C]$^{-1}$) for all data binned according to dominance by each of the 3 size groups (micro- [n = 26], nano- [n = 20] and pico-phytoplankton [n = 13]; for details, see 'Materials and methods'). Welch's *t*-test results are shown comparing the difference between the 3 size groups. Values in **bold** indicate significant correlations at p < 0.01

Dominant group	Size composition (%) Micro	Nano	Pico	K_C
Micro	56.4 (2.6)	28.9 (1.8)	14.6 (2.2)	21.8 (3.5)
Nano	23.2 (3.1)	58.5 (2.4)	18.4 (3.1)	16.7 (2.1)
Pico	11.0 (1.3)	35.1 (1.0)	53.8 (2.1)	22.1 (3.2)
p	**<0.001**	**<0.001**	**<0.001**	0.6

DISCUSSION

Studies are increasingly demonstrating that FRRF-based ETRs couple well with C-uptake rates (e.g. Lawrenz et al. 2013, Schuback et al. 2015), but that the exact relationship between rates varies with environmental condition (Lawrenz et al. 2013), as we also recently observed for waters of Ariake Bay (Zhu et al. 2016) and for our current study. Our study differs from many previous works examining variance of K_C (e.g. reviewed by Lawrenz et al. 2013) where C uptake was determined from ^{14}C uptake typically over 1–2 h incubations, and thus presumably closer to gross C uptake (GPP), whereas we used ^{13}C uptake over 24 h incubations (i.e. net primary production, NPP). This differentiation is important, as Halsey et al. (2010, 2011) noted that K_C measurements based on net C production measurements are more tightly coupled than those based on gross C production measurements across gradients of varying nutrient availability. In our current study, we observed that light appears to be most associated with deviation of K_C from the theoretical minimum value of 4 mol e^- (mol C)$^{-1}$ (Fig. 6), as previously observed for another region using the same approach (Ariake Bay, see Zhu et al. 2016); however, we further demonstrate

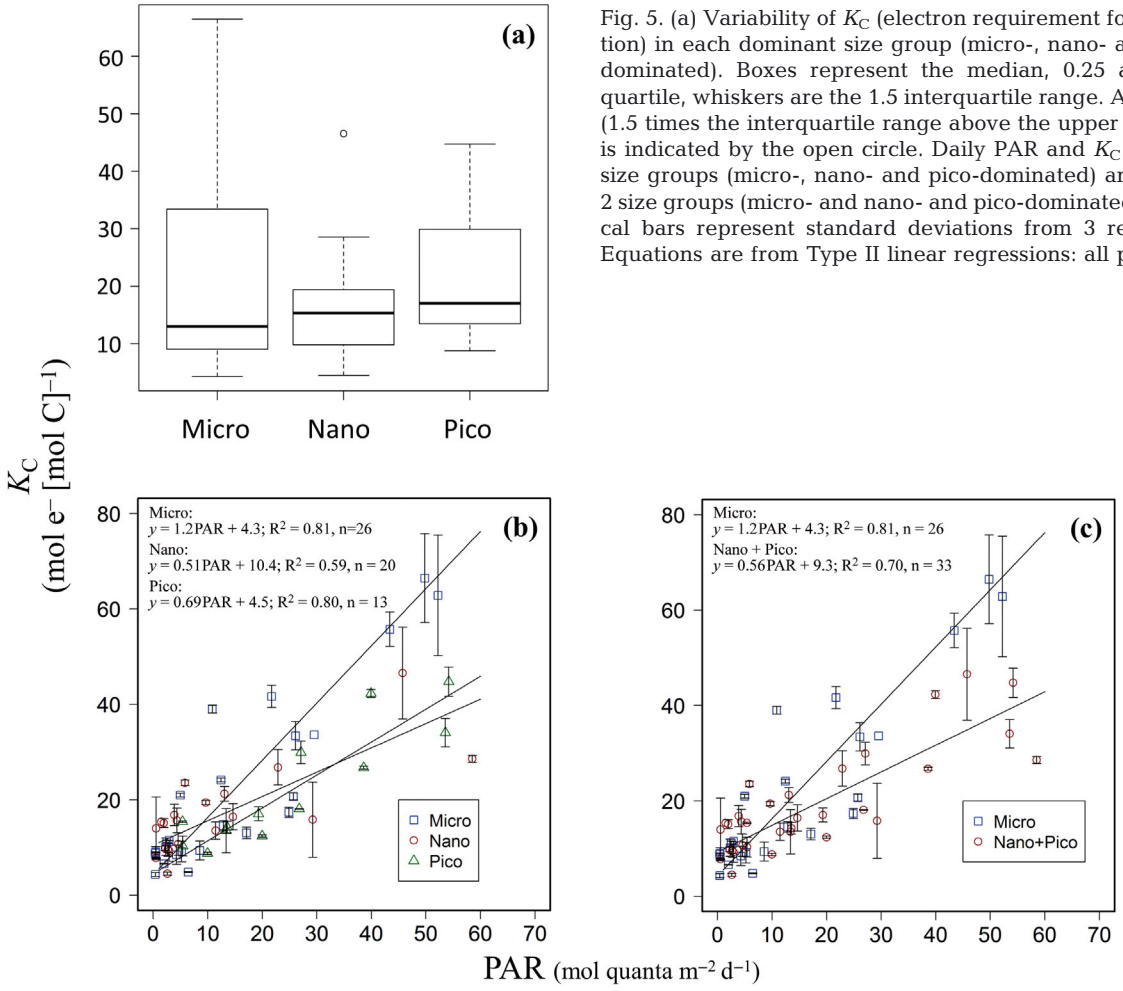

Fig. 5. (a) Variability of K_C (electron requirement for C-fixation) in each dominant size group (micro-, nano- and pico-dominated). Boxes represent the median, 0.25 and 0.75 quartile, whiskers are the 1.5 interquartile range. An outlier (1.5 times the interquartile range above the upper quartile) is indicated by the open circle. Daily PAR and K_C for (b) 3 size groups (micro-, nano- and pico-dominated) and (c) for 2 size groups (micro- and nano- and pico-dominated). Vertical bars represent standard deviations from 3 replicates. Equations are from Type II linear regressions: all p < 0.001

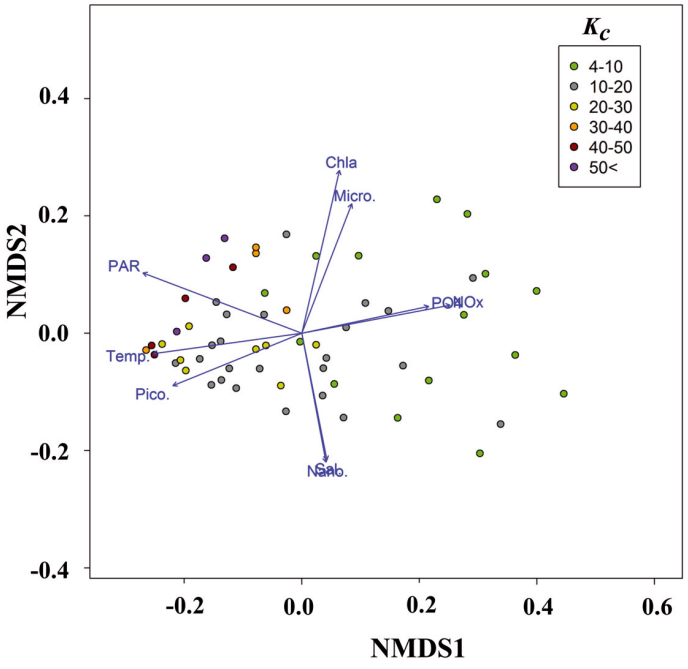

Fig. 6. Biplot of 2-dimensional non-metric multidimensional scaling (NMDS). Coloured labels are sampling points, blue arrows are environmental/community factors. Chla: chlorophyll *a*; Micro. (Nano., Pico.): micro-(nano-, pico-) phytoplankton; NO_x: nitrate + nitrite; PAR: photosynthetically active radiation; PO_4: phosphate; Sal: salinity; Temp.: temperature

that in fact phytoplankton taxonomic structure, which in part is inherently tied to changes in physico-chemical conditions (see also Suggett et al. 2006a), appears to be an important contributor to variability of K_C over broad scales. In the following sections, we discuss these findings and how they provide a means to estimate K_C (and hence net C uptake from FRRF) in the ECS and TS regions.

Light and phytoplankton community effects on K_C variability

Values of K_C for our current study (summer season in the eastern ECS and TS) varied from 1.0 to 66.5 mol e^- (mol C)$^{-1}$ (mean ± SD: 18.2 ± 16.6, n = 67). Whilst this range of values is somewhat higher than that recently reported for Ariake bay (2.3–26.6, Zhu et al. 2016), it is within that previously reported from a global assessment covering broad biogeographic environments (1.15–54.2 mol e^- [mol C]$^{-1}$, mean: 10.9 ± 6.91; Lawrenz et al. 2013), where higher values were characteristic of waters subjected to nutrient stress and/or limitation. As with many previous FRRF-based studies (Corno et al. 2006, Melrose et al. 2006, Suggett et al. 2006a, 2009a), some values for K_C lower than the theoretical minimum (4 mol e^- [mol C]$^{-1}$, see Kolber & Falkowski 1993) were observed, but only for deeper waters with extremely low light intensities. Low values for K_C (<4 mol e^- [mol C]$^{-1}$) have been observed in culture (2.68–3.79 mol e^- [mol C]$^{-1}$, Suggett et al. 2009a, Hoppe et al. 2015) and *in situ* (e.g. 0.24–2.46 mol e^- [mol C]$^{-1}$, Robinson et al. 2014), and generally considered an overestimation of C uptake and/or underestimation of ETR (Suggett et al. 2009a, Lawrenz et al. 2013) particularly when cyanobacteria are present (see Simis et al. 2012, Robinson et al. 2014). Furthermore, the lowest values of K_C we observed were all from deep waters where ambient light levels were lowest. As such, it is likely that low values of K_C may have been driven by inaccurate C uptake measurement (overestimation) for samples from low photic zones (Cullen 2001), or not accounting for inherent diurnal variability in n_{PSII} that may cause underestimation of ETR (Schuback et al. 2016). However, we cannot further discount possible additional overestimation of C uptake where these deeper (low light) samples were also incubated at higher temperatures than ambient as a result of on-deck incubations using surface water for temperature control. Here, average temperature differences between the upper mixed and deep layers (1 and 5% surface light depths) was ca. 8.5°C, which can cause as much as 40% overestimate of the C-uptake rate (Davison 1991).

K_C values in excess of 4 mol e^- (mol C)$^{-1}$ are reflective of ETRs that are decoupled from C fixation (Lawrenz et al. 2013), in particular as cellular demands for energy (ATP) and reductant (NADPH) from processes other than C fixation increase (see Suggett et al. 2009a, 2010). In our present study, we observed the decoupling of ETRs from C uptake in particular at high irradiances, also consistent with the recent observations across a broad range of biogeographic areas (Schuback et al. 2015, 2016), an Arctic fjord (Hancke et al. 2015) and a semi-closed embayment (Zhu et al. 2016). Intensity of the ambient light field appears to be a dominant environmental factor associated with decoupling of ETR from primary productivity (PP) in our study (Figs. 3d & 6). This outcome is perhaps not surprising.

Firstly, equilibration of isotopic label through cellular pools pushes the PP estimate towards net photosynthesis with longer incubations as recently-fixed ^{13}C is increasingly respired (i.e. dark loss; Eppley & Sharp 1975). The magnitude of loss can be very high, particularly at high irradiance, and can be dependent on nutrient status (Halsey et al. 2014), and thus potentially explain the irradiance-dependent increase

in K_C we observed. Secondly, mechanisms such as photoprotection act to dissipate electrons/consume O_2 without necessarily impacting on CO_2 once light intensity exceeds that required to saturate photochemistry (e.g. Schuback et al. 2015). Maximum turnover rates of the electron transport chain (ETC) require that excess excitation energy be dissipated as thermal energy in the PSII antenna (known as non-photochemical quenching, NPQ) in order to avoid photoinhibition. Indeed, NPQ has been observed to highly correlate with K_C/n_{PSII} (Schuback et al. 2015, 2016, 2017), which may result from the progressive photoinactivation of n_{PSII} with increasing irradiance (Behrenfeld et al. 1998), or the co-response to excess excitation pressure for both NPQ and K_C/n_{PSII} (Schuback et al. 2016). In order to account for any such changes in n_{PSII} (and simultaneously address whether use of a constant for n_{PSII} potentially introduced error into ETR and hence K_C), we repeated a diurnal analysis of relative $1/n_{PSII}$ as per Schuback et al. (2016). For this, we examined F_o/σ_{PSII} as the factor describing n_{PSII} stability (Oxborough et al. 2012). Results showed that differences in n_{PSII} with time of day were not significant for 7 of 12 cruises (Welch's *t*-test, Table S3 in the Supplement). Thus n_{PSII} remains somehow constant with time of day and does not exhibit very large diurnal variance in our study (Table S3), suggesting that other processes must account for our light dependency of K_C.

High electron transport (but low C assimilation) can be sustained via up-regulation of alternative electron flow after charge separation at PSII. For example, plastoquinol terminal oxidase uses electrons from the plastoquinone pool to reduce oxygen and thus protect PSII acceptors from high light damage (reviewed by Cardol et al. 2011). Electrons passed to PSI can be used to further reduce oxygen by Mehler activity (Mehler 1951, Roberty et al. 2014). As a result, C-fixation rates saturate with lower irradiances than ETRs (Mackey et al. 2008, Schuback et al. 2017) and hence decoupling between ETRs and C uptake would be expected to increase as irradiance continues to increase above that for light saturation (E_K). Consequently, on balance, photoprotective processes would likely provide a rationale as to why K_C often varies with light availability. However, it should be noted that our study considers daily-integrated ETR and P^C_B, and hence mechanisms acting to decouple these 2 rates (and hence K_C) must ultimately reflect the outcome of longer-term photo-acclimation processes.

Previous studies have indicated light-dependency of K_C from field evidence, where low light conditions are associated with lower K_C values (see Lawrenz et al. 2013), and from laboratory experiments on microalgae (Suggett et al. 2008, 2010, Brading et al. 2013). However, strong covariance of K_C with PAR was not demonstrated until Zhu et al. (2016) did so for Ariake Bay. That said, as compared to our previous observations (Zhu et al. 2016; their Fig. 9c), a relatively large proportion of variance for K_C could not be explained by PAR, notably at high daily PAR values (Fig. 3d), confirming that factors other than light regulation are also responsible for variations in K_C (e.g. Suggett et al. 2006a, Lawrenz et al. 2013, Schuback et al. 2015).

Adaptive differences in energy and reductant demands to maintain growth optima would explain observations of K_C variability within a relatively small range; specifically, previous laboratory experiments under controlled growth conditions report K_C with a range of ca. 5–15 across diatoms, flagellates and chlorophytes (Suggett et al. 2009a, Brading et al. 2013); these values remain lower than those reported for our natural samples (4.3 to 66.5 mol e^- [mol C]$^{-1}$), but generally within a similar range reported by Schuback et al. (2015, 2016) for a diatom and prymnesiophyte (ca. 6 to 20 mol e^- [mol C]$^{-1}$) assuming a value for $1/n_{PSII}$ of ca. 650 versus 1325 mol chl *a* (mol RCII)$^{-1}$ for iron-replete versus -limited eukaryotes (see Silsbe et al. 2015). Although the ECS is not under iron limitation, we observed a higher range of K_C than compared to those of Schuback et al. (2015, 2016) in the iron-limited Pacific. There are 2 main reasons that probably can explain this difference; firstly, we agree that the nutrient level could influence K_C value, and K_C will likely be elevated under conditions of nutrient stress/starvation (Lawrenz et al. 2013). However, both Schuback et al. (2015, 2016) and our studies (Zhu et al. 2016, this study) suggested that K_C appears primarily influenced by light intensity (presented as NPQ by Schuback et al. 2015, 2016); thus, the larger K_C values found in our surface data probably relate to the higher daily PAR included in this study (40–60 mol quanta m^{-2} d^{-1} vs. ca. 30 mol quanta m^{-2} d^{-1} in Schuback et al. 2015, 2016). Secondly, the different incubation time that the 2 studies applied may also cause our higher K_C value. Specifically, the longer incubating time (24 h, i.e. NPP) of our study than for Schuback et al. (2015, 2016) (3–4 h, i.e. GPP) probably resulted in our lower PP and thus higher K_C presented here. Our high values for K_C (>15–20 mol e^- [mol C]$^{-1}$) occur almost exclusively where PAR was highest (>20 mol quanta m^{-2} d^{-1}), reinforcing the notion of high light in moderating the cellular demands of energy/reductant (and the need to consume 'excess' electrons and/or O_2). However, most importantly this light-dependency is dif-

ferent for our f_{micro} compared to f_{nano} + f_{pico} fractions (Fig. 5c), whereby the higher linear regression slope for f_{micro} suggests that high light decoupling of ETRs and C uptake appears more severe for diatoms/dinoflagellates (Fuco- and Per-dominated communities) compared to nanoflagellates (Hex, But, Allo and chl *b*) and cyanobacteria-(Zea)-dominated communities.

Whilst higher values of K_C for f_{micro} would seem to contrast with previous observations where K_C typically remains low for diatom- (and flagellate)-dominated waters (e.g. Suggett et al. 2006a), we can potentially explain these higher values from 1 or more factors. Differences in light absorption efficiency and electron transport between phytoplankton groups no doubt enhance ETR_{RCII} variability to a certain degree (see Giannini & Ciotti 2016). The higher K_C values observed for larger phytoplankton in our study imply that energy transfer efficiency from photochemistry to biomass production is lower for large phytoplankton. However, the fact that highly effective photoprotection mechanisms appear to operate in both large (e.g. diatoms, especially for those living in dynamic waters; Lavaud et al. 2002, 2007, Hoppe et al. 2015) and small (Dimier et al. 2007, 2009) phytoplankton taxa, as well as highly conserved ETR(z) versus PAR(z) (Fig. 3a) across depths/campaigns in our study, would suggest that taxonomic differences associated with light harvesting (and importantly dissipation) did not likely contribute to the differences observed for K_C. Instead, differences in P_B^C (C fixation) appear to play a key role (Fig. 3b, Table 5).

Lower size-normalised photosynthetic rates for large-size phytoplankton have frequently been reported (Malone 1980, Montecino & Quiroz 2000, Bouman et al. 2005, Kameda & Ishizaka 2005, Tripathy et al. 2014, Barnes et al. 2015) and explained by lower surface-to-volume ratio of larger phytoplankton reducing nutrient uptake efficiency (Sunda & Huntsman 1997) and light absorption (Marra et al. 2007). Such constraints are thus compounded by nutrient limitation (Riegman et al. 1993, Pedersen & Borum 1996). Whilst f_{micro} was generally dominant in waters with lower salinity and higher nutrients (Cluster B, Fig. 4a), nutrient concentrations were still overall very low (NO_x^-: ~0.5 µM; PO_4^{3-}: ~0.09 µM) and at concentrations in this region where phytoplankton generally appear to experience nutrient stress (Liu et al. 2013). However, higher values of P_B^C are more typical for large phytoplankton when under nutrient-replete conditions (Cermeño et al. 2005). Such overall nutrient-limited (starving) conditions may thus also explain the somewhat contrasting observations here compared to our recent study in Ariake Bay (Zhu et al. 2016) where nutrients were replete; specifically, phytoplankton in Ariake Bay exhibited higher P_B^C values (and thus lower K_C and lower regression slope value of $K_C(z)$ versus PAR(z); Zhu et al. 2016) under similar light intensity as for our current study.

In addition, the high abundance of cyanobacteria in the f_{nano} + f_{pico} may have driven an overall lower value for K_C for this fraction compared to the f_{micro} (Robinson et al. 2014; see also Simis et al. 2012). Clearly, resolving which of these factors is at play is currently beyond our study and further highlights that more controlled experiments are required to disentangle the potentially confounding role of (non-steady state) environmental conditions and taxonomy upon K_C. Although we cannot fully resolve the mechanisms driving the values of K_C within our current study, our data still demonstrate a clear role of taxonomy (or at least pigment group as in our study) in better accounting for variance of K_C across spatially and/or temporally separated samples.

Table 5. Means (± SE) of electron transfer rate (ETR, mmol e^- [mg chl *a*]$^{-1}$ d^{-1}), P^B (chl *a* normalised primary productivity; mgC [mg chl *a*]$^{-1}$ d^{-1}) and K_C (electron requirement for C-fixation; mol e^- [mol C]$^{-1}$) in the upper mixed layer of 2 dominant size classes of phytoplankton (micro, n = 11; nano + pico, n = 13). Welch's *t*-test results are presented for examining the significant difference of parameters between 2 groups. **Bold** indicates a significant correlation at $p < 0.05$

Dominant group	ETR	P_B^C	K_C
Micro	91 (10)	35.2 (3.0)	35.0 (5.7)
Nano + Pico	109 (10)	46.8 (2.1)	29.2 (2.6)
p	0.3	**0.01**	0.4

Uncertainty assessment of the linear relationship between PAR and K_C

As with previous K_C-focussed studies, a large number of assumptions are employed, in particular for the FRRF-based ETRs (Lawrenz et al. 2013, Schuback et al. 2015). Whilst the strong co-variation between K_C and light we observed here provides a potentially promising means to easily retrieve K_C from future FRRF data, it is critical to first evaluate the possible error propagation via the *a priori* assumptions used. Notably, the assumed constant value for n_{PSII} of 0.0038 for picoplankton is higher than that reported by Suggett et al. (2004) for *Aureococcus* and *Pycnococcus* (ca. 2 µm in diameter and a mean value of 0.0013 mol RCII [mol chl *a*]$^{-1}$). Also, the correction method for σPSII is based on absorption spectra

rather than fluorescence excitation spectra (see also Suggett et al. 2010), which in the latter case likely better accounts for the proportion of all light absorbed by PSII especially for cyanobacteria (Suggett et al. 2004, Moore et al. 2006). In the case of our parallel ^{13}C-uptake measurements, we acknowledge that the lack of dissolved organic C (DOC) measurement in this study will underestimate P_B^C and thus overestimate K_C by ca. 2–50%, particularly at high irradiance (Thornton 2014).

To consider such uncertainties, we therefore re-examined our light–K_C relationship by randomly introducing error estimates to each step. Firstly, we assumed that a fraction of between 0 and 30% of pico-phytoplankton is indeed eukaryotic (e.g. species of *Pycnococcus* and *Aureococcus*) rather than cyanobacteria (*Synechococcus*), which would reduce n_{PSII} by ca. 0–20%. A random number (chosen by R function runif()) within this 0–20% range of n_{PSII} was therefore subtracted from the original value to simulate such uncertainty. Second, we assumed our σ_{PSII} correction factor F would be overestimated ca. 0–20% because of using absorption spectra over fluorescence excitation spectra in weighting of σ_{PSII} for cyanobacteria (Moore et al. 2006), and thus generated a random number within this range. Third, in order to account for the underestimation of PP caused by the lack of DOC measurements, the ratio of dissolved PP to particulate PP (REP) was considered to be a value of 5–30% based on the nutrient conditions of the study area (Thornton 2014). Particularly, 10–30% of the REP was added to P_B^C incubated under high light (i.e. 100 and 50% surface light), whereas 5–10% error was added to P_B^C for all other samples accounting for a reduced REP proportion under lower irradiances (Parker & Armbrust 2005, Thornton et al. 2014).

Uncertainty was thus determined as

$$n_{PSII\,simulated} = n_{PSII\,calculated} - n_{PSII\,calculated} \cdot x1\% \quad (14)$$

$$F_{simulated} = F_{calculated} - F_{calculated} \cdot x2\% \quad (15)$$

$$P^C_{B\,simulated} = P^C_{B\,measured} + P^C_{B\,measured} \cdot y\% \quad (16)$$

where $x1$%, $x2$% and y% are evenly distributed random numbers added to the parameters for accounting uncertainty of each.

Determination of uncertainty (simulation) was repeated 100 times. The resultant K_C was calculated for each simulated ETR and P_B^C and compared against daily PAR, as per the original data. We then calculated the mean ± SD of the correlation coefficient (R^2), slope and intercept from the entire 100 simulations combined, as 0.63 ± 0.04, 0.54 ± 0.04 and 4.6 ± 0.3, respectively (i.e. K_C = 0.54 × PAR + 4.6 with R^2 = 0.63, $p < 0.01$). In comparison to our original data (K_C = 0.85 × PAR + 6.5 with R^2 = 0.66), the extent of covariance that can be explained by a linear model is broadly equivalent, but as expected, changing the absolute terms with the ETR and ^{13}C equations significantly changes the slope. However, importantly in the case of our study, this uncertainty analysis confirms that a linear relationship between light and K_C is robust and highly repeatable depending on the choice of assumption used to generate the electron transport and C uptake rates. That said, future studies will need to move beyond the use of these assumptions and the inherent uncertainty that is introduced.

Towards improved *in situ* application of FRRF-based K_C and NPP estimates

Our analyses here for the ECS and TS (as well as that previously for Ariake Bay; Zhu et al. 2016) have shown that variance of K_C can be reconciled with that of light availability. This outcome appears in agreement with previous data analyses from Lawrenz et al. (2013), who showed that K_C measurements from coastally influenced waters such as European shelf seas and the Baltic/Gulf of Finland could be modelled, in part, against optical depth and *in situ* light attenuation. Our data also confirm that knowledge of additional physico-chemical conditions is needed to effectively improve the robustness of these models (Fig. 4b). Lawrenz et al. (2013) highlighted that a comprehensive description of physico-chemical conditions (temperature, salinity, nutrients etc.) is required to best explain variance of K_C. Whilst our analysis using taxonomic-based clusters provided only slightly improved co-variance of K_C versus light, it arguably provides a more simplistic but powerful means to potentially predict K_C and hence NPP. Specifically, knowledge of fewer variables (in our case, phytoplankton size fractions based on pigment groups, as opposed to a salinity and nutrients that predominantly separated our stations) is required to bin K_C and light. Clearly, the semi-continuous measurement of pigment groups needed to ensure the validity of FRRF across highly physically dynamic waters is not trivial. High-throughput particle sensors may provide some means to retrieve phytoplankton size structure (Álvarez et al. 2011, 2014). However, our size-based approach used knowledge of pigment groups. Thus parallel continuous measurements of light absorption (Ciotti et al. 2002, Wang et al. 2015), or better yet multispectral

FRRF discrimination (Silsbe et al. 2015), may provide a means to identify taxonomic groups and their influence upon K_C.

In determining ETR_{RCII} and hence K_C (via ^{13}C-based daily integrated NPP estimates), we used several assumptions. Specifically, algorithms describing (1) the spectral conversion of σ_{PSII} from the FRRF LEDs relative to the *in situ* light fields (Suggett et al. 2009b), and (2) taxonomic weighting of n_{PSII}. The role of these assumptions in potentially influencing ETR has been reviewed extensively previously (e.g. Suggett et al. 2009b, 2010, Robinson et al. 2014). Even so, despite employing these assumptions, we demonstrated strong co-variance between K_C and environmental (and biological) factors, thus providing a robust means to retrieve NPP across from future FRRF measurements for this region. In fact, such assumptions may not even be required where new FRRF-based ETR models can remove the need for knowledge of n_{PSII} (Oxborough et al. 2012, Silsbe et al. 2015, Murphy et al. 2017; see also Schuback et al. 2015), and relatively small variability of the correction factor for σPSII with depth (Fig. S2 in the Supplement), possibly suggesting that a single conserved correction factor could be employed with relatively little loss of accuracy. Such an outcome supports, at least in part, the notion that conversion of absorbed energy to net C fixation exhibits limited variability in the absence of non-photochemical quenching (Silsbe et al. 2016). Regardless of these future improvements, our study provides further evidence that FRRF-based ETRs can be reconciled with independent C-uptake measurements, but for the first time through knowledge of phytoplankton groups. In doing so, we have produced a predictive algorithm for K_C for this ocean region, opening possibilities of using FRRF-based platforms to examine C fluxes with improved resolution.

Acknowledgements. We thank the captain, officers and crew of TV 'Nagasaki Maru' for their assistance during onboard sampling and measurements. Many thanks to Dr. Koji Suzuki for measuring HPLC data. The earlier version of the manuscript greatly benefited from the critical reading by Drs. Akiko Mizuno and Egil Sakshaug. We thank 4 anonymous reviewers for their very constructive comments and suggestions. This research was supported by the Global Change Observation Mission-Climate (GCOM-C) Project of the Japan Aerospace Exploration Agency and partially supported by the Japan Society for the Promotion of Science KAKENHI (JP26241009) and Zhejiang Provincial Natural Science Foundation of China (LQ16C030004). The contribution by D.J.S. was supported by an Australian Research Council Future Fellowship (FT130100202); the contribution by J.G. was supported by the National Aeronautics and Space Administration (NNX16AD40G).

LITERATURE CITED

Álvarez E, López-Urrutia Á, Nogueira E, Fraga S (2011) How to effectively sample the plankton size spectrum? A case study using FlowCAM. J Plankton Res 33: 1119–1133

Álvarez E, Moyano M, López-Urrutia Á, Nogueira E, Scharek R (2014) Routine determination of plankton community composition and size structure: a comparison between FlowCAM and light microscopy. J Plankton Res 36:170–184

Barnes MK, Tilstone GH, Smyth TJ, Widdicombe CE and others (2015) Drivers and effects of *Karenia mikimotoi* blooms in the western English Channel. Prog Oceanogr 137:456–469

Behrenfeld MJ, Prasil O, Kolber ZS, Babin M, Falkowski PG (1998) Compensatory changes in photosystem II electron turnover rates protect photosynthesis from photoinhibition. Photosynth Res 58:259–268

Bouman H, Platt T, Sathyendranath S, Stuart V (2005) Dependence of light-saturated photosynthesis on temperature and community structure. Deep Sea Res I 52: 1284–1299

Brading P, Warner ME, Smith DJ, Suggett DJ (2013) Contrasting modes of inorganic carbon acquisition amongst *Symbiodinium* (Dinophyceae) phylotypes. New Phytol 200:432–442

Cardol P, Forti G, Finazzi G (2011) Regulation of electron transport in microalgae. Biochim Biophys Acta Bioenerg 1807:912–918

Cermeño P, Estévez-Blanco P, Maranón E, Fernández E (2005) Maximum photosynthetic efficiency of size-fractionated phytoplankton assessed by ^{14}C uptake and fast repetition rate fluorometry. Limnol Oceanogr 50: 1438–1446

Cheah W, McMinn A, Griffiths FB, Westwood KJ and others (2011) Assessing Sub-Antarctic Zone primary productivity from fast repetition rate fluorometry. Deep Sea Res II 58:2179–2188

Ciotti AM, Lewis MR, Cullen JJ (2002) Assessment of the relationships between dominant cell size in natural phytoplankton communities and the spectral shape of the absorption coefficient. Limnol Oceanogr 47:404–417

Cleveland JS, Weidemann AD (1993) Quantifying absorption by aquatic particles: a multiple scattering correction for glass-fiber filters. Limnol Oceanogr 38:1321–1327

Corno G, Letelier RM, Abbott MR, Karl DM (2006) Assessing primary production variability in the North Pacific subtropical gyre: a comparison of fast repetition rate fluorometry and ^{14}C measurements. J Phycol 42:51–60

Cullen JJ (2001) Primary production methods. In: Steele JH, Turekian K, Thorpe SA (eds) Encyclopedia of ocean sciences. Elsevier, Amsterdam, p 2277–2284

Davison IR (1991) Environmental effects on algal photosynthesis: temperature. J Phycol 27:2–8

Dimier C, Corato F, Saviello G, Brunet C (2007) Photophysiological properties of the marine picoeukaryote *Picochlorum* RCC 237 (Trebouxiophyceae, Chlorophyta). J Phycol 43:275–283

Dimier C, Brunet C, Geider R, Raven J (2009) Growth and photoregulation dynamics of the picoeukaryote *Pelagomonas calceolata* in fluctuating light. Limnol Oceanogr 54:823–836

Eppley RW, Sharp JH (1975) Photosynthetic measurements in the central North Pacific: the dark loss of carbon in 24 h incubations. Limnol Oceanogr 20:981–987

Fujiki T, Hosaka T, Kimoto H, Ishimaru T, Saino T (2008)

In situ observation of phytoplankton productivity by an underwater profiling buoy system: use of fast repetition rate fluorometry. Mar Ecol Prog Ser 353:81–88

Giannini MFC, Ciotti M (2016) Parameterization of natural phytoplankton photo-physiology: effects of cell size and nutrient concentration. Limnol Oceanogr 61:1495–1512

Gong GC, Wen YH, Wang BW, Liu GJ (2003) Seasonal variation of chlorophyll *a* concentration, primary production and environmental conditions in the subtropical East China Sea. Deep Sea Res II 50:1219–1236

Guo X, Miyazawa Y, Yamagata T (2006) The Kuroshio onshore intrusion along the shelf break of the East China Sea: the origin of the Tsushima Warm Current. J Phys Oceanogr 36:2205–2231

Halsey KH, Jones BM (2015) Phytoplankton strategies for photosynthetic energy allocation. Annu Rev Mar Sci 7: 265–297

Halsey KH, Milligan AJ, Behrenfeld MJ (2010) Physiological optimization underlies growth rate-independent chlorophyll-specific gross and net primary production. Photosynth Res 103:125–137

Halsey KH, Milligan AJ, Behrenfeld MJ (2011) Linking time-dependent carbon-fixation efficiencies in *Dunaliella tertiolecta* (Chlorophyceae) to underlying metabolic pathways. J Phycol 47:66–76

Halsey KH, Milligan AJ, Behrenfeld MJ (2014) Contrasting strategies of photosynthetic energy utilization drive lifestyle strategies in ecologically important picoeukaryotes. Metabolites 4:260–280

Hama T, Miyazaki T, Ogawa Y, Iwakuma T, Takahashi M, Otsuki A, Ichimura S (1983) Measurement of photosynthetic production of a marine phytoplankton population using a stable ^{13}C isotope. Mar Biol 73:31–36

Hancke K, Dalsgaard T, Sejr MK, Markager S, Glud RN (2015) Phytoplankton productivity in an Arctic fjord (West Greenland): estimating electron requirements for carbon fixation and oxygen production. PLOS ONE 10: e0133275

Hirata T, Aiken J, Hardman-Mountford N, Smyth T, Barlow R (2008) An absorption model to determine phytoplankton size classes from satellite ocean colour. Remote Sens Environ 112:3153–3159

Hoppe CJ, Holtz LM, Trimborn S, Rost B (2015) Ocean acidification decreases the light-use efficiency in an Antarctic diatom under dynamic but not constant light. New Phytol 207:159–171

Ichikawa H, Beardsley RC (2002) The current system in the Yellow and East China Seas. J Oceanogr 58:77–92

Jassby AD, Platt T (1976) Mathematical formulation of the relationship between photosynthesis and light for phytoplankton. Limnol Oceanogr 21:540–547

Kameda T, Ishizaka J (2005) Size-fractionated primary production estimated by a two-phytoplankton community model applicable to ocean color remote sensing. J Oceanogr 61:663–672

Kolber ZS, Falkowski PG (1993) Use of active fluorescence to estimate phytoplankton photosynthesis in situ. Limnol Oceanogr 38:1646–1665

Kolber ZS, Prášil O, Falkowski PG (1998) Measurements of variable chlorophyll fluorescence using fast repetition rate techniques: defining methodology and experimental protocols. Biochim Biophys Acta 1367:88–106

Kromkamp JC, Dijkman NA, Peene J, Simis SG, Gons HJ (2008) Estimating phytoplankton primary production in Lake IJsselmeer (The Netherlands) using variable fluorescence (PAM-FRRF) and C-uptake techniques. Eur J Phycol 43:327–344

Lavaud J, Van Gorkom HJ, Etienne AL (2002) Photosystem II electron transfer cycle and chlororespiration in planktonic diatoms. Photosynth Res 74:51–59

Lavaud J, Strzepek RF, Kroth PG (2007) Photoprotection capacity differs among diatoms: possible consequences on the spatial distribution of diatoms related to fluctuations in the underwater light climate. Limnol Oceanogr 52:1188–1194

Lawrenz E, Silsbe G, Capuzzo E, Ylöstalo P and others (2013) Predicting the electron requirement for carbon fixation in seas and oceans. PLOS ONE 8:e58137

Liu HC, Shih CY, Gong GC, Ho TY, Shiah FK, Hsieh CH, Chang J (2013) Discrimination between the influences of river discharge and coastal upwelling on summer microphytoplankton phosphorus stress in the East China Sea. Cont Shelf Res 60:104–112

Mackey KR, Paytan A, Grossman AR, Bailey S (2008) A photosynthetic strategy for coping in a high-light, low-nutrient environment. Limnol Oceanogr 53:900–913

Malone TC (1980) Size-fractionated primary productivity of marine phytoplankton In: Falkowski PG (ed) Primary productivity in the sea. Springer, New York, NY, p 301–319

Marra JF (2015) Ocean productivity: a personal perspective since the first Liege Colloquium. J Mar Syst 147:3–8

Marra JF, Trees CC, O'reilly JE (2007) Phytoplankton pigment absorption: a strong predictor of primary productivity in the surface ocean. Deep Sea Res I 54:155–163

Mehler AH (1951) Studies on reactions of illuminated chloroplasts. I. Mechanism of the reduction of oxygen and other Hill reagents. Arch Biochem Biophys 33: 65–77

Melrose DC, Oviatt CA, O'Reilly JE, Berman MS (2006) Comparisons of fast repetition rate fluorescence estimated primary production and ^{14}C uptake by phytoplankton. Mar Ecol Prog Ser 311:37–46

Mino Y, Matsumura S, Lirdwitayaprasit T, Fujiki T, Yanagi T, Saino T (2014) Variations in phytoplankton photophysiology and productivity in a dynamic eutrophic ecosystem: a fast repetition rate fluorometer-based study. J Plankton Res 36:398–411

Montecino V, Quiroz D (2000) Specific primary production and phytoplankton cell size structure in an upwelling area off the coast of Chile (30° S). Aquat Sci 62:364–380

Moore CM, Suggett DJ, Hickman AE, Kim YN and others (2006) Phytoplankton photoacclimation and photoadaptation in response to environmental gradients in a shelf sea. Limnol Oceanogr 51:936–949

Morimoto A, Takikawa T, Onitsuka G, Watanabe A, Moku M, Yanagi T (2009) Seasonal variation of horizontal material transport through the eastern channel of the Tsushima Straits. J Oceanogr 65:61–71

Murphy CD, Ni G, Li G, Barnett A and others (2017) Quantitating active photosystem II reaction center content from fluorescence induction transients. Limnol Oceanogr Methods 15:54–69

Murtagh F, Legendre P (2014) Ward's hierarchical agglomerative clustering method: Which algorithms implement Ward's criterion? J Classif 31:274–295

Ning XR, Liu ZL, Cai YM, Fang M, Chai F (1998) Physico-biological oceanographic remote sensing of the East China Sea: satellite and in situ observations. J Geophys Res 103:21623–21635

Oxborough K, Moore CM, Suggett DJ, Lawson T, Chan HG, Geider RJ (2012) Direct estimation of functional PSII reaction center concentration and PSII electron flux on a volume basis: a new approach to the analysis of Fast Rep-

etition Rate fluorometry (FRRf) data. Limnol Oceanogr Methods 10:142–154
Parker MS, Armbrust E (2005) Synergistic effects of light, temperature, and nitrogen source on transcription of genes for carbon and nitrogen metabolism in the centric diatom *Thalassiosira pseudonana* (Bacillariophyceae). J Phycol 41:1142–1153
Pedersen MF, Borum J (1996) Nutrient control of algal growth in estuarine waters. Nutrient limitation and the importance of nitrogen requirements and nitrogen storage among phytoplankton and species of macroalgae. Mar Ecol Prog Ser 142:261–272
Ralph PJ, Wilhelm C, Lavaud J, Jakob T, Petrou K, Kranz SA (2010) Fluorescence as a tool to understand changes in photosynthetic electron flow regulation. In: Suggett DJ, Prášil O, Borowitzka MA (eds) Chlorophyll *a* fluorescence in aquatic sciences: methods and applications. Springer, Dordrecht, p 75–89
R Core Team (2014) R: A language and environment for statistical computing. R Foundation for Statistical Computing, Vienna. www.R-project.org
Riegman R, Kuipers BR, Noordeloos AA, Witte HJ (1993) Size-differential control of phytoplankton and the structure of plankton communities. Neth J Sea Res 31: 255–265
Roberty S, Bailleul B, Berne N, Franck F, Cardol P (2014) PSI Mehler reaction is the main alternative photosynthetic electron pathway in *Symbiodinium* sp., symbiotic dinoflagellates of cnidarians. New Phytol 204:81–91
Robinson C, Suggett DJ, Cherukuru N, Ralph PJ, Doblin MA (2014) Performance of fast repetition rate fluorometry based estimates of primary productivity in coastal waters. J Mar Syst 139:299–310
Schuback N, Schallenberg C, Duckham C, Maldonado MT, Tortell PD (2015) Interacting effects of light and iron availability on the coupling of photosynthetic electron transport and CO_2-assimilation in marine phytoplankton. PLOS ONE 10:e0133235
Schuback N, Flecken M, Maldonado MT, Tortell PD (2016) Diurnal variation in the coupling of photosynthetic electron transport and carbon fixation in iron-limited phytoplankton in the NE subarctic Pacific. Biogeosciences 13: 1019–1035
Schuback N, Hoppe CJ, Tremblay JÉ, Maldonado MT, Tortell PD (2017) Primary productivity and the coupling of photosynthetic electron transport and carbon fixation in the Arctic Ocean. Limnol Oceanogr 62:898–921
Silsbe GM, Oxborough K, Suggett DJ, Forster RM and others (2015) Toward autonomous measurements of photosynthetic electron transport rates: an evaluation of active fluorescence-based measurements of photochemistry. Limnol Oceanogr Methods 13:138–155
Silsbe GM, Behrenfeld MJ, Halsey KH, Milligan AJ, Westberry TK (2016) The CAFE model: a net production model for global ocean phytoplankton. Global Biogeochem Cycles 30:1756–1777
Simis SG, Huot Y, Babin M, Seppälä J, Metsamaa L (2012) Optimization of variable fluorescence measurements of phytoplankton communities with cyanobacteria. Photosynth Res 112:13–30
Siswanto E, Ishizaka J, Yokouchi K (2006) Optimal primary production model and parameterization in the eastern East China Sea. J Oceanogr 62:361–372
Suggett DJ, Macintyre HL, Geider RJ (2004) Evaluation of biophysical and optical determinations of light absorption by photosystem II in phytoplankton. Limnol Oceanogr Methods 2:316–332
Suggett DJ, Maberly SC, Geider RJ (2006a) Gross photosynthesis and lake community metabolism during the spring phytoplankton bloom. Limnol Oceanogr 51:2064–2076
Suggett DJ, Moore CM, Marañón E, Omachi C, Varela RA, Aiken J, Holligan PM (2006b) Photosynthetic electron turnover in the tropical and subtropical Atlantic Ocean. Deep Sea Res II 53:1573–1592
Suggett DJ, Warner ME, Smith DJ, Davey P, Hennige S, Baker NR (2008) Photosynthesis and production of hydrogen peroxide by *Symbiodinium* (Pyrrhophyta) phylotypes with different thermal tolerances. J Phycol 44:948–956
Suggett DJ, MacIntyre HL, Kana TM, Geider RJ (2009a) Comparing electron transport with gas exchange: parameterising exchange rates between alternative photosynthetic currencies for eukaryotic phytoplankton. Aquat Microb Ecol 56:147–162
Suggett DJ, Moore CM, Hickman AE, Geider RJ (2009b) Interpretation of fast repetition rate (FRR) fluorescence: signatures of phytoplankton community structure versus physiological state. Mar Ecol Prog Ser 376:1–19
Suggett DJ, Moore CM, Geider RJ (2010) Estimating aquatic productivity from active fluorescence measurements. In: Suggett DJ, Prášil O, Borowitzka MA (eds) Chlorophyll *a* fluorescence in aquatic sciences: methods and applications. Springer, Dordrecht, p 103–127
Sunda WG, Huntsman SA (1997) Interrelated influence of iron, light and cell size on marine phytoplankton growth. Nature 390:389–392
Suzuki R, Ishimaru T (1990) An improved method for the determination of phytoplankton chlorophyll using N, N-dimethylformamide. J Oceanogr Soc Jpn 46:190–194
Thornton DC (2014) Dissolved organic matter (DOM) release by phytoplankton in the contemporary and future ocean. Eur J Phycol 49:20–46
Tripathy SC, Ishizaka J, Fujiki T, Shibata T, Okamura K, Hosaka T, Saino T (2010) Assessment of carbon-and fluorescence-based primary productivity in Ariake Bay, southwestern Japan. Estuar Coast Shelf Sci 87:163–173
Tripathy SC, Pavithran S, Sabu P, Naik R, Noronha S, Bhaskar P, Kumar NA (2014) Is primary productivity in the Indian Ocean sector of Southern Ocean affected by pigment packaging effect? Curr Sci 107:1019–1026
Uitz J, Claustre H, Morel A, Hooker SB (2006) Vertical distribution of phytoplankton communities in open ocean: an assessment based on surface chlorophyll. J Geophys Res 111:C08005
Van Heukelem L, Thomas CS (2001) Computer-assisted high-performance liquid chromatography method development with applications to the isolation and analysis of phytoplankton pigments. J Chromatogr A 910:31–49
Vidussi F, Claustre H, Manca BB, Luchetta A, Marty JC (2001) Phytoplankton pigment distribution in relation to upper thermocline circulation in the eastern Mediterranean Sea during winter. J Geophys Res 106:19939–19956
Wang S, Ishizaka J, Yamaguchi H, Tripathy SC and others (2014) Influence of the Changjiang River on the light absorption properties of phytoplankton from the East China Sea. Biogeosciences 11:1759–1773
Wang S, Ishizaka J, Hirawake T, Watanabe Y, Zhu Y, Hayashi M, Yoo S (2015) Remote estimation of phytoplankton size fractions using the spectral shape of light absorption. Opt Express 23:10301–10318
Zhu Y, Ishizaka J, Tripathy SC, Wang S, Mino Y, Matsuno T, Suggett DJ (2016) Variation of the photosynthetic electron transfer rate and electron requirement for daily net carbon fixation in Ariake Bay, Japan. J Oceanogr 72: 761–776

Editorial responsibility: Steven Lohrenz, New Bedford, Massachusetts, USA

Submitted: December 5, 2016; Accepted: August 17, 2017
Proofs received from author(s): September 21, 2017